ISSN: 1074-133X Vol 31 No. 4s (2024)

Joint Effects of Velocity and Thermal Wall Slips on Steady, Laminar, MHD Jeffrey-Nano Fluid Flow Over a Non-Linearly Stretching of a Flat surface

B. Chandrasekhar^{1,2}, M. Chenna Krishna Reddy³

¹ Department of Mathematics, JNTUH College of Engineering, Hyderabad, Telangana State, India.

² Department of Mathematics, Vardhaman College of Engineering, Hyderabad, Telangana State, India.

³ Department of Mathematics, University College of Science, Osmania University, Hyderabad, Telangana State, India.

*Corresponding author Email address: shekmaths10@gmail.com

Article History:

Received: 17-05-2024

Revised: 23-06-2024

Accepted: 11-07-2024

Abstract: The effect of Thermophoresis and Brownian motion on the time-dependent (steady) magnetohydrodynamic boundary layer Jeffrey fluid flow of a nonlinearly stretching sheet in the existence of nanoparticles is investigated in this research. Nonlinear partial differential equations serve as the governing equations in the system. Then, applying appropriate similarity transformations, these equations are reduced into ordinary differential equations. To get numerical solutions to the resulting differential equations, the shooting method is employed. This article presents an in-velocity analysis of a variety of engineering parameters, including the Jeffrey fluid parameter, Brownian motion parameter, Thermophoresis parameter, Stretching sheet parameter, Prandtl number, Lewis number, Velocity slip parameter, and Thermal slip parameter, as well as numerical values for heat and mass transfer. Finally, it is established that the numerical findings are fully compatible with the published results. This kind of scientific study has a variety of applications, including energy conservation, microprocessor cooling, and equipment longevity.

Keywords: Jeffrey fluid; Nanofluid; MHD; Non-linearly stretching sheet; Velocity and thermal wall slips.

1. Introduction

Non-Newtonian fluids are considered better than viscous fluids at present. Newtonian fluids are not (or non-Newtonian materials). Most lubricants, lacquers, oils, cosmetics, clay laminates and colloidal suspension solutions are examples. Due to its numerous uses in the industry, engineering, physiology and biosciences, non-Newtonian fluids have acquired popularity. No fluid model describes correctly the characteristics of all fluids. The results of this research have been directly related with non-Newtonian fluids. The second, third, and fourth grade models as well as the general Burgers models are available. The Jeffrey model is one of these models [1]. The fluid of Jeffrey exhibits both relaxation and delays. Vajravelu et al. [2] examined the convective flow, heat transfer and mass transfer on a vertical stretching sheet using the Ostwald-de-Waele fluid. Naranjan and colleagues have been investigating the radiative heat and mass transport of a Jeffrey fluid over a stretch sheet[3]. Jena and her colleagues [4] investigated fluid flow over a stretch sheet including MHD processes, heat production and absorption. The homotopy for heat transfer on a radially stretching convective surface in an unstable flow employing Jeffrey nanofluid has been examined by Sreelakshmi et al. [5]. Das et al. [7] studied Jeffrey fluid and radiation-induced fusion heat transfer radiation MHD slip flow. As a consequence of binary chemical reaction and energy activation Shafique et al. [8] calculated the flow

ISSN: 1074-133X Vol 31 No. 4s (2024)

of spinning Jeffrey fluid. Hayat et al. [9] have investigated the multi-dimensional (MHD), radially stretching, Jeffrey fluid flow. In the presence of convective border circumstances, Shehzad et al. [10] studied Jeffrey's stagnation point flow. In a range of thermal flux conditions Abbasi et al. [11] examined Jeffrey's Multi-dimensional (MHD) fluid flow. The Jeffrey fluid peristaltic flow was examined by Tripathi et al. [12]. When homogenous heterogeneous processes are present, Farooq et al. [13] examine the characteristics of Jeffrey fluid flow. Zin et al. [14] examined the transfer of heat using the Jeffrey nanofluid spinning MHD stream. Hayat et al. [15] explored a nonlinear expanded surface Jeffrey fluid for the use of MHD. The nanoflow generated by the angled stretching cylinders and the resultant temperature stratification was investigated by Ramzan et al. [16]. The continuing fluid flow of Jeffrey between spinning cylinders has been described by Shifang et al. [17]. Hayat et al. [18] studied fluid flow of Jeffrey in homogenous heterogeneous processes between two stretchy spinning discs. The flow of Jeffrey fluid was studied using a stretching sheet by Narayana et al. [19]. Juohn's nanofluid flow was discovered in a laboratory environment by Hayat et al. [20]. Shehzad et al. [21] investigated the effects of convective heat and concentration conditions in magnetohydrodynamic flow of Jeffrey fluid with nanoparticles.

Following that, the current work contributes to find the numerical simulations of Jeffery-nanofluid flow were performed using a non-linearly stretching sheet. Furthermore, Magnetic field, velocity and thermal wall slips effects are included. Differential equations are used to solve the flow issue (ODE's). A system of ODE's is rendered dimensionless (through appropriate variables). To resolve the system of ODE's, the Runge-Kutta method is combined with the Shooting Method. The next sections demonstrate the findings of these ODE's for velocity, temperature, and nanoparticle concentration profiles. Additionally, physical quantities are evaluated using tabular data. The structure of this research work is the mathematical solutions for the control equations are provided in Section 3. Section 4 compares the current numerical results to those obtained in the absence of a Jeffrey fluid, Magnetic field, velocity and thermal wall slip effects by Rana and Bhargava et al. [22]. Section 5 explores flow parameter engineering parameter values utilising physical factors such as velocity, temperature, nanoparticle concentration, wall shear stress, rate of energy transfer and species transfers. Finally, the final arguments are presented in Section 6.

2. Mathematical Analysis

Fig. 1 depicts a schematic depiction of the physical model and coordinates system, as well as a coordinates system. For this research work, the following assumptions are made.

- 1. Let us consider the flow of a nanofluid through a flat sheet that coincides with the plane y = 0 and is restricted to the region y > 0.
- 2. The flow is constant, incompressible, laminar, and two-dimensional boundary layer flow. It is produced as a result of non-linear stretching of the sheet, which is induced by the application of two equal and opposing pressures along the x-axis at the same time.
- 3. When the origin is held constant, the sheet is then stretched with a velocity $u_w = ax^n$, where a denotes constant, n denotes nonlinear stretching parameter, and x is the coordinate along the stretching surface, which varies nonlinearly with distance from the slit.

ISSN: 1074-133X Vol 31 No. 4s (2024)

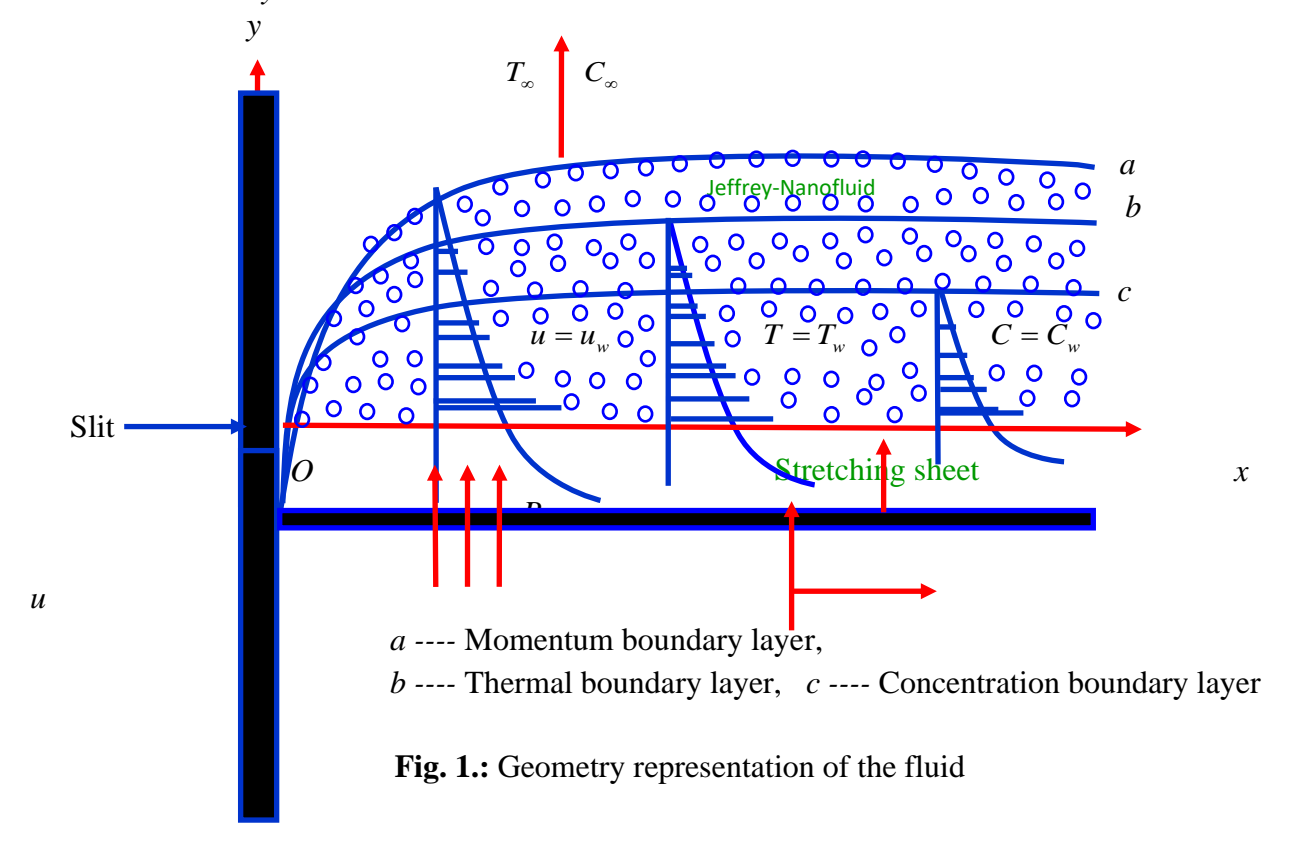
- 4. Normally, a variable magnetic field B(x) will be provided to the surface of the sheet while the magnetic field induced is minimal and may be justified for MHD flow at the small magnetic Reynolds number.
- 5. The gradient of pressure and external forces are not taken into consideration.
- 6. The temperature and concentration of the stretching surface, T_w and C_w , are kept at constant values, and these values are considered to be higher than the temperature and concentration of the surrounding environment, T_∞ and T_∞ , which are maintained at constant values.
- 7. It is well known that the constitutive equations for a Jeffrey fluid are given by (Nadeem and Akbar [23])

$$\tau = -pI + S \tag{1}$$

Where
$$S = \frac{\mu}{1+\gamma} \left\{ R_1 + \gamma_1 \left[\frac{\partial R_1}{\partial t} + \overline{V} \cdot \nabla \right] R_1 \right\}$$
 (2)

In Eq. (2),
$$R_1$$
 is the Rivlin-Ericksen tensor defined by $R_1 = (\nabla \overline{V}) + (\nabla \overline{V})'$ (3)

Based on the above assumptions, the fundamental steady-state conservation of mass, momentum, thermal energy, and nanoparticles equations for Jeffrey-Nanofluids can be written in Cartesian coordinates *x* and *y* as:



Continuity Equation:

$$\left(\frac{\partial u}{\partial x}\right) + \left(\frac{\partial v}{\partial y}\right) = 0\tag{4}$$

ISSN: 1074-133X Vol 31 No. 4s (2024)

Momentum Equation:

$$u\left(\frac{\partial u}{\partial x}\right) + v\left(\frac{\partial u}{\partial y}\right) = v\left(\frac{1}{1+\gamma}\right) \left\{\frac{\partial^2 u}{\partial y^2} + \gamma_1 \left[u\left(\frac{\partial^3 u}{\partial x \partial y^2}\right) + v\left(\frac{\partial^3 u}{\partial y^3}\right) - \left(\frac{\partial u}{\partial x}\frac{\partial^2 u}{\partial y^2}\right) + \left(\frac{\partial u}{\partial y}\frac{\partial^2 u}{\partial x \partial y}\right)\right]\right\} - \left(\frac{\sigma B_o^2}{\rho_f}\right) u \quad (5)$$

Equation of thermal energy:

$$u\left(\frac{\partial T}{\partial x}\right) + v\left(\frac{\partial T}{\partial y}\right) = \alpha_m \left(\frac{\partial^2 T}{\partial y^2}\right) + \left[\frac{(\rho C)_p}{(\rho C)_f}\right] \left\{D_B\left(\frac{\partial C}{\partial y}\right)\left(\frac{\partial T}{\partial y}\right) + \left(\frac{D_T}{T_\infty}\right)\left(\frac{\partial T}{\partial y}\right)^2\right\}$$
(6)

Equation of nanoparticle concentration:

$$u\left(\frac{\partial C}{\partial x}\right) + v\left(\frac{\partial C}{\partial y}\right) = D_B\left(\frac{\partial^2 C}{\partial y^2}\right) + \left(\frac{D_T}{T_\infty}\right)\left(\frac{\partial^2 T}{\partial y^2}\right) \tag{7}$$

Where
$$\alpha_m = \frac{k_m}{(\rho C)_f}$$
.

Subject to the boundary conditions for Jeffrey-nano fluid flow with velocity and thermal wall slip effects are

$$u = u_{w} = ax^{n} + L\left(\frac{\partial u}{\partial y}\right), \quad v = 0, \quad T = T_{w} + Z\left(\frac{\partial T}{\partial y}\right), \quad C = C_{w} \quad at \quad y = 0$$

$$u \to 0, \quad v \to 0, \quad T \to T_{\infty}, \quad C \to C_{\infty} \quad as \quad y \to \infty$$

$$(8)$$

The following similarity variables are introduced for solving governing equations (5)-(7) as

$$\eta = y \left(\sqrt{\frac{a(n+1)}{2\nu}} \right) x^{\frac{n-1}{2}}, \quad u = ax^n f'(\eta), \quad v = -\left(\sqrt{\frac{a\nu(n+1)}{2}} \right) x^{\frac{n-1}{2}} \left(f(\eta) + \left(\frac{n-1}{n+1} \right) \eta f'(\eta) \right), \\
\theta(\eta) = \frac{T - T_{\infty}}{T_{w} - T_{\infty}}, \quad \phi(\eta) = \frac{C - C_{\infty}}{C_{w} - C_{\infty}}$$
(9)

Using Eq. (9), the fundamental Eqs. (5) to (7) become

$$f''' + (1+\gamma) \left\{ ff'' - \left(\frac{2n}{n+1}\right) f'^{2} \right\} + \beta \left\{ f''^{2} - ff'''' \right\} - (1+\gamma) Mf' = 0$$
 (10)

$$\theta'' + \Pr f \theta' + \Pr Nb\theta' \phi' + \Pr Nt\theta'^2 = 0 \tag{11}$$

$$2Nb\phi'' + NbLef\phi' + 2Nt\theta'' = 0 \tag{12}$$

and the corresponding boundary conditions (9) become

$$\begin{cases}
f = 0, & f' = 1 + \lambda f''(0), & \theta = 1 + \delta \theta'(0), & \phi = 1 & \text{at } \eta = 0 \\
f' \to 0, & \theta \to 0, & \phi \to 0 & \text{as } \eta \to \infty
\end{cases}$$
(13)

where the involved physical parameters are defined as

ISSN: 1074-133X Vol 31 No. 4s (2024)

$$\Pr = \frac{v}{\alpha}, M = \frac{\sigma B_o^2 x}{\rho_f a}, Le = \frac{v}{D_B}, Nb = \frac{\left(\rho C\right)_p D_B (C_w - C_\infty)}{\left(\rho C\right)_f v}, Nt = \frac{\left(\rho C\right)_p D_T (T_w - T_\infty)}{\left(\rho C\right)_f v T_\infty},$$

$$\lambda = L\sqrt{\frac{a}{v}}, \delta = Z\sqrt{\frac{a}{v}}, \beta = a\gamma_1$$

$$(14)$$

It is important to note that when n=1 and Nb, Nt are equal to zero in Eqs. (11) and (12), this boundary value problem reduces to the classical problem of flow and heat and mass transfer due to a stretching surface in a viscous fluid (the boundary value problem reduces to the classical problem (The boundary value problem reduces to the classical problem for n=1 and becomes ill-posed and is of no physical significance). It should be noted that Eq. (10) and the boundary conditions (13) with n=0 are the traditional Blasius flat-plate flow issue, and that the author of this paper has carried out a thorough numerical analysis of that problem in his previous work. For the linearly stretching boundary problem (i.e., n=1) the exact solution for f is $f(\eta) = 1 - e^{-\eta}$, first obtained by Crane [22] and this exact solution is unique, while for the nonlinearly stretching boundary problem (i.e., $n \ne 1$) there is no exact solution. The parameters of engineering interest in heat and mass transport problems are the Skin-friction coefficient (Cf), local Nusselt number (Nu_x) and the Sherwood number (Sh_x) are defined as

$$Cf = \left(\frac{1}{1+\gamma}\right) \frac{\tau_{w}}{\rho_{f} U^{2}} \quad \text{where} \quad \tau_{w} = \frac{\mu}{1+\gamma} \left\{ \left(\frac{\partial u}{\partial y}\right) + \gamma_{1} \left[\frac{\partial^{2} u}{\partial x \partial y} + u \left(\frac{\partial^{2} v}{\partial x^{2}}\right) + v \left(\frac{\partial^{2} u}{\partial x^{2}}\right) \right] \right\}_{y=0}$$

$$\Rightarrow \left(\sqrt{\operatorname{Re}_{x}}\right) Cf = \left(\frac{1}{1+\gamma}\right) \left\{ f''(0) + \beta \left[f'(0)f''(0) - f(0)f'''(0)\right] \right\}$$

$$(15)$$

$$Nu_{x} = \frac{xq_{w}}{k_{m}(T_{w} - T_{\infty})} \quad \text{where } q_{w} = -k_{m}(T_{w} - T_{\infty})x^{\frac{n-1}{2}} \left(\sqrt{\frac{a(n+1)}{2\nu}}\right)\theta'(0)$$

$$\Rightarrow Nu_x = -x^{\frac{n+1}{2}} \left(\sqrt{\frac{a(n+1)}{2\nu}} \right) \theta'(0) \tag{16}$$

$$Sh_{x} = \frac{xq_{m}}{D_{B}\left(C_{w} - C_{\infty}\right)} \quad \text{where } q_{m} = -D_{B}\left(C_{w} - C_{\infty}\right)x^{\frac{n-1}{2}} \left(\sqrt{\frac{a(n+1)}{2\nu}}\right) \phi'(0)$$

$$\Rightarrow Sh_x = -x^{\frac{n+1}{2}} \left(\sqrt{\frac{a(n+1)}{2\nu}} \right) \phi'(0) \tag{17}$$

ISSN: 1074-133X Vol 31 No. 4s (2024)

3. Numerical Solutions by Runge-Kutta Method with Shooting Technique

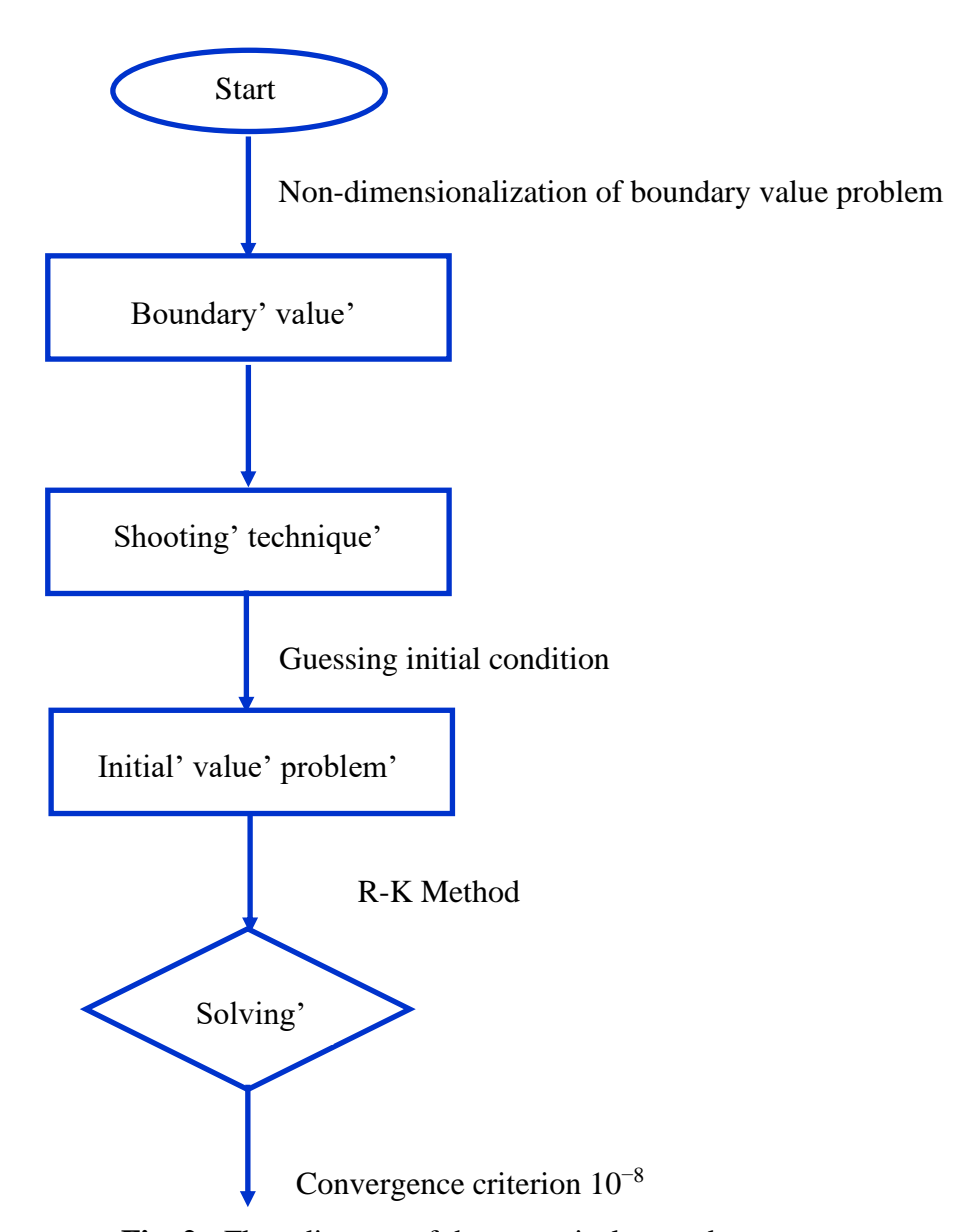


Fig. 2.: Flow diagram of the numerical procedure

In order to solve the system of ordinary differential equations (10)-(12) with their corresponding initial and boundary conditions (13) numerically, the domain $[0, \infty)$ has been substituted by the bounded domain $[0, \eta_{\infty}]$ where η_{∞} is a suitable finite real number that should be chosen in such a way that the solution satisfies the domain. Also (10)-(12) form a highly nonlinear coupled initial boundary value problem of third and second order ODEs. For this reason, (10)-(12) have been reduced to a system of seven initial problems of the first order of seven unknowns from the following the supposition in

$$f = y_1, f' = y_2, f'' = y_3, f''' = y_4, \theta = y_5, \theta' = y_6, \phi = y_7, \phi' = y_8$$
 (18)

Thus, we develop the most effective numerical technique in line with the fourth order Runge-Kutta shooting technique. The symbolic software MAPLE is used to obtain the numerical solution. To solve

ISSN: 1074-133X Vol 31 No. 4s (2024)

this system, we require seven initial conditions whereas we have only four initial conditions for f(0), f'(0), $\theta(0)$ and $\phi(0)$, while the other three f''(0), $\theta'(0)$ and $\phi'(0)$ were not given; hence, we employ numerical shooting technique where these three initial conditions are guessed to produce the required three ending boundary conditions. During the mathematical simulation, the step size is to be $\Delta \eta = 0.001$ in order to acquire results. The criterion of convergence is 10^{-8} . The subsequent procedure is visualized through Fig. 2.

4. Program Code Validation

Table-1.: Comparison of present Nusselt number results with published Nusselt number results of Rana and Bhargava [22] for various values of n, Nt and Nb when $\gamma \to \infty$, $\gamma_1 = \lambda = \delta = 0$

n	Nt	Prese	ent $-\theta'(0)$ re	Published $-\theta'(0)$ results of			
		11000			Rana a	and Bhargav	/a [22]
		Nb = 0.5	Nb = 1.0	Nb = 2.5	Nb = 0.5	Nb = 1.0	Nb = 2.5
0.2	0.1	0.50966231	0.26684112	0.03025587	0.5160	0.2775	0.0303
0.2	0.3 0.44863001		0.23516647	0.02644721	0.4533	0.2427	0.0265
	0.5	0.38223112	0.20966466	0.02336222	0.3999	0.2135	0.0234
	0.1	0.47223568	0.41995033	0.36854178	0.4864	0.4282	0.3786
3.0	0.3	0.41882014	0.21988745	0.02493226	0.4282	0.2293	0.0251
	0.5	0.36488201	0.20199556	0.02198852	0.3786	0.2020	0.0221
	0.1	0.46930277	0.24833147	0.02826659	0.4799	0.2581	0.0283
10.0	0.3	0.41996203	0.21996442	0.02463327	0.4227	0.2263	0.0247
	0.5	0.36952214	0.19954482	0.02135865	0.3739	0.1996	0.0214

Table-2.: Comparison of present Sherwood number results with published Sherwood number results of Rana and Bhargava [22] for various values of n, Nt and Nb when $\gamma \to \infty$, $\gamma_1 = \lambda = \delta = 0$

n	Nt	Prese	ent $-\phi'(0)$ re	Published $-\phi'(0)$ results of			
			, ()	Rana and Bhargava [22]			
		Nb = 0.5	Nb = 1.0	Nb = 2.5	Nb = 0.5	Nb = 1.0	Nb = 2.5
0.2	0.1	0.89912546	0.94111527	0.94226578	0.9012	0.9413	0.9493
0.2	0.3	0.82951324	0.93855402	0.94982201	0.8395	0.9394	0.9571
	0.5	0.80472362	0.93300124	0.96221555	0.8048	0.9429	0.9642
	0.1	0.84443015	0.76992488	0.73200184	0.8445	0.7785	0.7379
3.0	0.3	0.77806695	0.86992031	0.89233478	0.7785	0.8792	0.8997
	0.5	0.72285621	0.86993211	0.89331751	0.7379	0.8793	0.9056
	0.1	0.82459970	0.86953144	0.87855213	0.8323	0.8722	0.8812
10.0	0.3	0.75582314	0.86011788	0.87844121	0.7654	0.8662	0.8873
	0.5	0.71993022	0.86234487	0.88930015	0.7238	0.8656	0.8930

ISSN: 1074-133X Vol 31 No. 4s (2024)

Table-3.: Comparison of present Nusselt number results with published Nusselt number results of Rana and Bhargava [22] for various values of Pr, n and Le when $\gamma \to \infty$, $\gamma_1 = \lambda = \delta = 0$

Pr		Prese	ent $-\theta'(0)$ re	Published $-\theta'(0)$ results of			
	n	11000	(*)	Rana and Bhargava [22]			
		Le = 2.0	Le = 10.0	Le = 25.0	Le = 2.0	Le = 10.0	Le = 25.0
0.7	0.2	0.31889234	0.29863314	0.28922154	0.3299	0.3042	0.2982
0.7	0.5	0.31986624	0.28996031	0.28922130	0.3216	0.2965	0.2906
	3.0	0.29844215	0.27995124	0.26844102	0.3053	0.2812	0.2757
	0.2	0.38751637	0.27933164	0.24866230	0.3999	0.2835	0.2569
2.0	0.5	0.38952261	0.26933157	0.24770547	0.3930	0.2778	0.2517
	3.0	0.36844201	0.25633647	0.23822014	0.3786	0.2661	0.2410
	0.2	0.21885421	0.04996321	0.03385147	0.2248	0.0547	0.0345
7.0	0.5	0.21998674	0.04963117	0.03178412	0.2261	0.0546	0.0328
	3.0	0.21988542	0.04886233	0.03086215	0.2288	0.0537	0.0319

For checking of program code validation, the present the results of Nusselt and Sherwood numbers are compared with the published results of Rana and Bhargava [22] in tables 1, 2, 3 and 4 respectively for various values of Pr, n, Le, Nb and Nt at $\gamma \to \infty$, $\gamma_1 = \lambda = \delta = 0$. From these tables it is observed that, there is an excellent correlation has been achieved with the earlier results of Rana and Bhargava [22].

Table-4.: Comparison of present Sherwood number results with published Sherwood number results of Rana and Bhargava [22] for various values of Pr, n and Le when $\gamma \to \infty$, $\gamma_1 = \lambda = \delta = 0$

Pr		Prese	ent $-\phi'(0)$ re	Published $-\phi'(0)$ results of			
	n		, (1)	Rana and Bhargava [22]			
		Le = 2.0	Le = 10.0	Le = 25.0	Le = 2.0	Le = 10.0	Le = 25.0
0.7	0.2	0.80592231	2.30885322	3.81877245	0.8132	2.3198	3.8262
0.7	0.5	0.78662487	2.28995417	3.79885412	0.7965	2.2959	3.8005
	3.0	0.75930014	2.23966521	3.73985524	0.7630	2.2464	3.7471
	0.2	0.79966548	2.41889230	3.94778221	0.8048	2.4207	3.9547
2.0	0.5	0.77855301	2.26844512	3.91872234	0.7826	2.2778	3.9245
	3.0	0.72999314	2.32998555	3.85944751	0.7379	2.3324	3.8616
	0.2	1.01025513	2.61955402	4.11823345	1.0114	2.6202	4.1223
7.0	0.5	0.97744102	2.57955418	4.08895223	0.9808	2.5871	4.0909
	3.0	0.90899523	2.50988314	4.01855234	0.9185	2.5194	4.0224

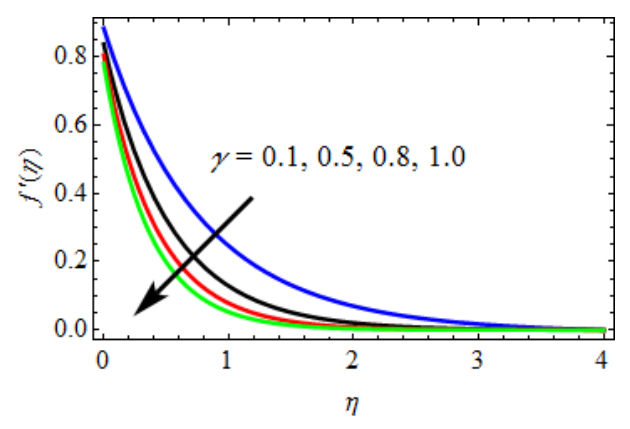
5. Results and Discussion

This section is prepared to study the impact of pertinent parameters namely Magnetic field parameter (M), Prandtl number (Pr), Jeffrey fluid material parameter (γ) , Stretching sheet parameter (n), Velocity slip parameter (λ) , Brownian motion parameter (Nb), Thermophoresis parameter (Nt), Thermal slip parameter (δ) , Deborah number (β) and Lewis parameter (Le) on velocity field components, temperature distributions and nanoparticle concentration profiles which are displayed graphically in Figs.: Fig. 3, Fig. 4, Fig. 5, Fig. 6, Fig. 7, Fig. 8, Fig. 9, Fig. 10, Fig. 11, Fig. 12, Fig. 13, Fig. 14 and

ISSN: 1074-133X Vol 31 No. 4s (2024)

the numerical values of Skin-friction, Nusselt and Sherwood number coefficients for the different values of the above said parameters are offered in tables: Table-5, Table-6 and Table-7.

- The impact of γ on velocity profiles is shown in Fig. 3. When the increase in γ is significant, it can be seen that the fluid velocity and boundary layer thickness both drop significantly. This is done in order to prevent things from speeding up since a slower recovery process leads in a longer relaxing period, which results in a thicker border layer.
- Fig. 4 depicts the difference in the stretching parameter (n) values for various non-linear stretching parameters as shown by the velocity profiles in this figure. The conclusion that can be taken from this result is that the velocity profiles get flatter as the quantity of n rises. In other words, when the non-linear stretching parameter n is increased, the thickness of the momentum barrier layer will decrease as well.



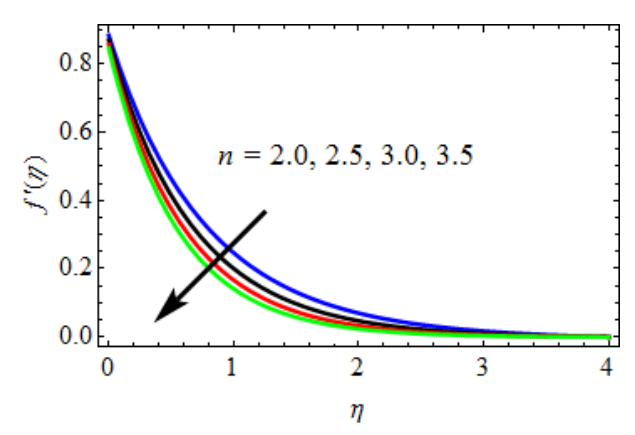


Fig. 3. γ influence on velocity profiles $f'(\eta)$

Fig. 4. *n* influence on velocity profiles $f'(\eta)$

- The intensity of the magnetic field in Fig. 5 has an impact on the velocity profiles of the particles. It has been observed that the magnetic parameter has an inverse relationship with the velocity parameter. A force known as the Lorentz force is generated when one increases the value of the magnetic parameter. In contrast to the fluid particle's mobility, the production of this force results in the generation of a resistive force. As a consequence, the velocity of the vehicle drops.
- As the fluid travels through an area of lower-than-average velocity, the streamwise velocity of the fluid (which is represented by the velocity slip parameter (λ)) is shown in Fig. 6. The relative velocity of the fluid falls as the stretched sheet travels at a quicker rate. As a result of the fact that the velocity slip parameter decreases with regard to the nanofluid velocity, this is true.
- The temperature change induced by the Prandtl number (Pr) on the fluid is shown in Fig. 7. As the value of Pr increases, the gradient of the fluid's temperature becomes less pronounced. The momentum diffusivity grows as Pr increases, while the thermal diffusivity becomes less important as Pr increases, as seen in the graph below. The fluid velocity must be sufficiently high in order to allow heat transfer to occur. A faster heat dissipation rate and smaller boundary layer thicknesses are produced as a consequence of this phenomenon.

ISSN: 1074-133X Vol 31 No. 4s (2024)

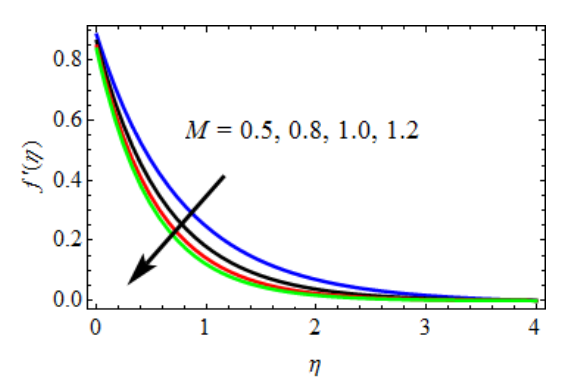


Fig. 5. *M* influence on velocity profiles $f'(\eta)$

From Figs. 8 and 9, it can be seen that the effect of the Brownian motion parameter, Nb, on temperature (θ) and concentration is shown (ϕ). As predicted, regular heat transfer fluid boundary layer profiles have the same form as non-regular heat transfer fluid boundary layer profiles. A rise in the boundary layer temperature occurs as a result of an increase in the Brownian motion parameter (Nb). In general, increasing the Nb parameter raises the nanoparticle volume fraction profile, as indicated by the symbol. Particle deposition onto the surface is thought to contribute to the drop in concentrations observed in Fig. 9, but it is also believed that Brownian motion has a warming effect on the boundary layer. Thermal conduction may be enhanced by either the Brownian motion of nanoparticles or microconvection of fluid that surrounds individual nanoparticles. The direct impact is more frequent. This is an excellent point. It seems that for smaller particles, Brownian motion is strong, and the parameter Nb will have high values. However, it is also obvious that Brownian motion has a large impact on both the temperature and concentration profiles of the particles.

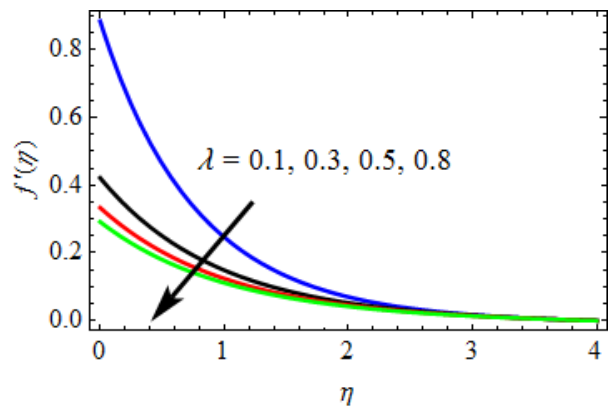


Fig. 6. λ influence on velocity profiles

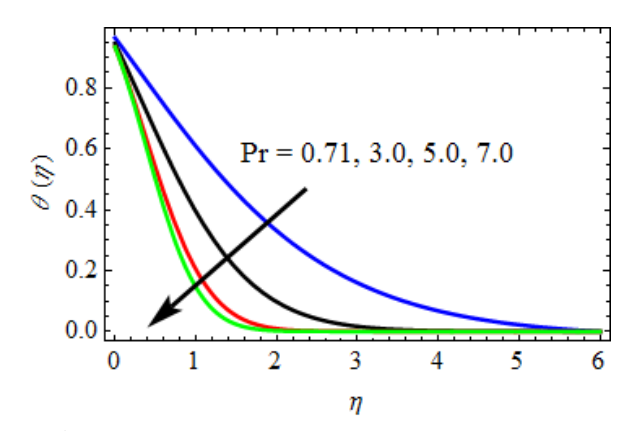
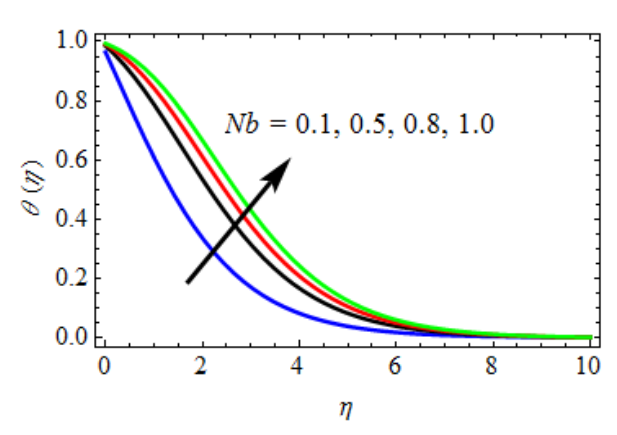


Fig. 7. Pr influence on temperature profiles

Fig. 10 and Fig. 11 show typical patterns for temperature and concentration depending on the Thermophoretic parameter (*Nt*) values. Using the Thermophoretic parameter (*Nt*) in this research, it was found that raising both fluid temperature and nanoparticle concentration is possible. In instances when the Prandtl number (Pr) and Lewis number (*Le*) are low, thermal conductivity (Thermophoresis) is used to warm the boundary layer (*Le*). When *Nt* rises, heat transmission and mass transfer both decreases.

ISSN: 1074-133X Vol 31 No. 4s (2024)



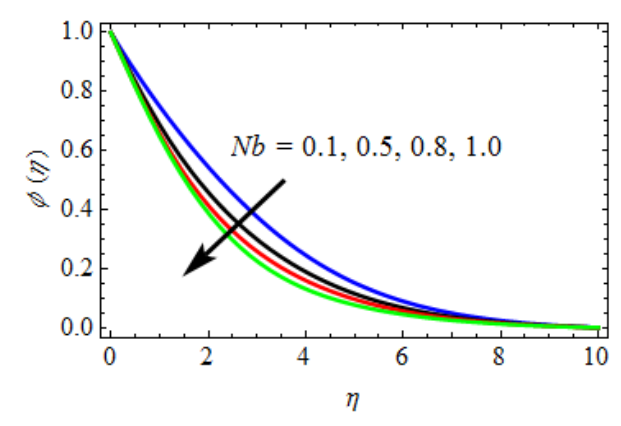


Fig. 8. *Nb* influence on temperature profiles

Fig. 9. *Nb* influence on nanoparticle concentration profiles

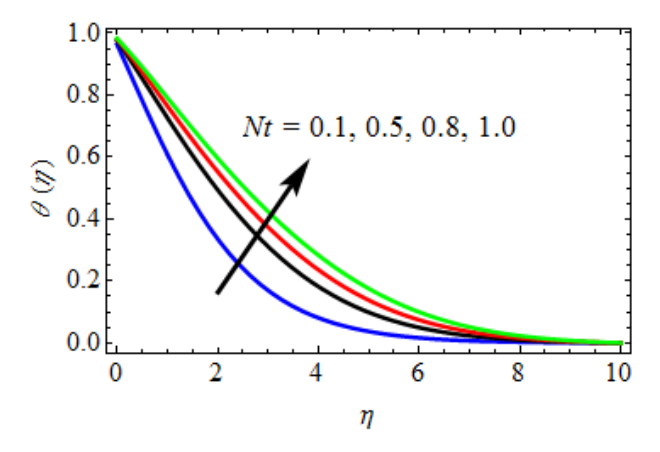
Fig. 12 depicts the correlation between nanoparticle concentration and the nanofluid Lewis number (*Le*). This is a Lewis number, and the Lewis number describes the ratio of the heat and mass diffusivity for a dimensionless nanofluid. Increasing the value of *Le* results in a substantial reduction in the nanoparticle volume percentage

Table-5.: Numerical values of skin-friction coefficient (*Cf*) for variations of M, γ , n, β , Pr, Nb, Nt, Le, δ and λ

			, ,	, n, p,		,	- ,			
M	γ	n	β	Pr	Nb	Nt	Le	δ	λ	Cf
0.5	0.1	2.0	0.1	0.71	0.1	0.1	0.1	0.1	0.1	1.6802214567
0.8										1.4503362154
1.0										1.3260012457
1.2										1.3053310214
	0.5									1.6235542389
	0.8									1.5831124512
	1.0									1.5586632112
		2.5								1.6132045887
		3.0								1.5862344512
		3.5								1.5563021247
			0.5							1.7236554879
			0.8							1.7560322478
			1.0							1.7782204421
				3.0						1.4863324451
				5.0						1.3587702121
				7.0						1.3069234457
					0.5					1.7130026584
					0.8					1.7320622583
					1.0					1.7782100215
						0.5				1.7236544852
						0.8				1.7403264558
						1.0				1.7830265514
							0.5			1.6325002137
							0.8			1.5930726454
							1.0			1.5763002984
								0.5		1.6230059125
								0.8		1.5930222365

ISSN: 1074-133X Vol 31 No. 4s (2024)





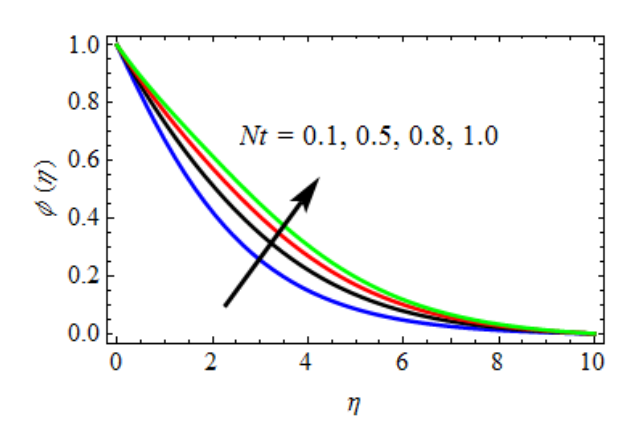


Fig. 10. Nt influence on temperature profiles

Fig. 11. *Nt* influence on nanoparticle concentration profiles

- The curve variations in the dimensionless temperature profiles are seen in Fig. 13 is demonstrated by the effect of the thermal slip parameter (δ) on the thermodynamic cycle. The temperature profiles have been clearly demonstrated to increase when rewards for outcomes are increased. As the value of the thermal slip parameter increases, the thermal boundary layer thickness decreases.
- In Fig. 14, you can see how the Deborah number (β) may affect the velocity profiles in different directions. The boundary layer thickness and fluid velocity will both rise when β is increased. It is because increasing the number of fewer increases the surface's resistance to fluid motion, which causes more fluid flow in the area where the surface is stretched.
- Table-5 shows the numerical values of Skin-friction coefficient (*Cf*) for variations in values of the engineering parameters such as, M, γ , n, β , Pr, Nb, Nt, Le, δ and λ . From this table, it is observed that the Skin-friction coefficient is increasing with rising values of Nb, Nt, β while it is decreasing with increasing values of M, γ , Pr, Le, n, δ and λ .

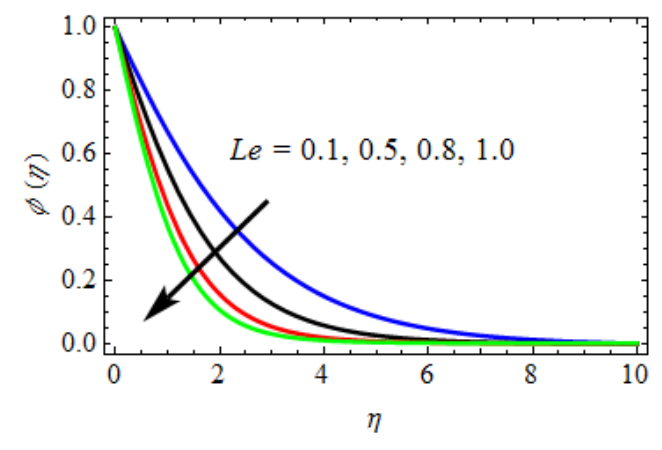


Fig. 12. *Le* influence on nanoparticle concentration profiles

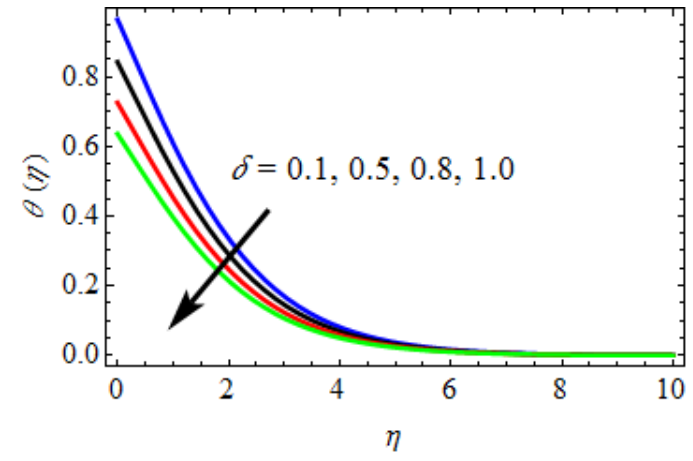


Fig. 13. δ influence on temperature profiles

ISSN: 1074-133X Vol 31 No. 4s (2024)

- The numerical values of rate of heat transfer coefficient in terms of Nusselt number are displayed in Table-6 for different values of Pr, Nb, Nt and δ . The rate of heat transfer coefficient is gradually rising with increasing values of Nb, Nt, while the reverse effect is observed in increasing values of Pr and δ .
- The effects of *Nb*, *Nt* and *Le* on the rate of mass transfer coefficient or in terms Sherwood number coefficient are discussed in Table-7. From this table, it is observed that the rate of mass transfer coefficient is increasing with increasing values of *Nb* and decreasing with increasing values of *Nt* and *Le*.

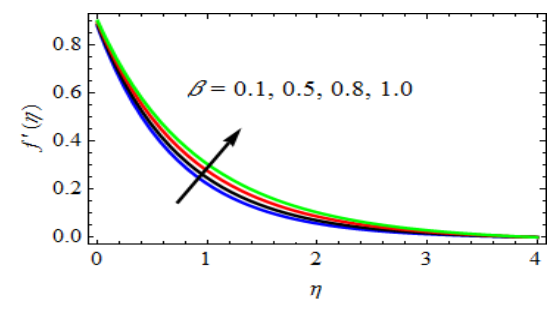


Fig. 14. β influence on velocity profiles

Table-6.: Numerical values of rate of heat transfer coefficient for different values of Pr, Nb, Nt and δ

Pr	Nb	Nt	δ	rate of heat transfer coefficient
0.71	0.1	0.1	0.1	0.8633215448
3.00				0.6533294125
5.00				0.6022451213
7.00				0.5863314552
	0.5			0.9032655487
	0.8			0.9352215626
	1.0			0.9532214578
		0.5		0.9133562487
		0.8		0.9402315486
		1.0		0.9603226545
			0.5	0.8031542232
			0.8	0.7621432120
			1.0	0.7432659124

Table-7.: Numerical values of rate of mass transfer coefficient for various values of Nb, Nt and Le

Nb	Nt	Le	rate of mass transfer coefficient
0.1	0.1	0.1	0.9532114651
0.5			0.9130026587
0.8			0.8923145466
1.0			0.8736620145
	0.5		0.9823100126
	0.8		1.0532240216
	1.0		1.0860322145
		0.5	0.9023665120
		0.8	0.8823001546
		1.0	0.8532261457

ISSN: 1074-133X Vol 31 No. 4s (2024)

6. Conclusions:

In this research, a viscous, incompressible MHD boundary layer with Brownian motion and Thermophoresis are being studied on a non-linearly stretched sheet for a stable and viscous boundary layer in a compressible medium. For the most part, this study is dedicated to solving nonlinear coupled ordinary differential equations using numerical techniques. Variables that are examined include many factors, and numerical data is provided in graphs and tables based on these results. The following details are also available:

- Velocity profile rises with the increment in the Thermophoresis (Nt), Brownian motion (Nb) and Deborah number (β).
- The velocity distribution is decreasing function of Magnetic field parameter (M), Jeffrey fluid material parameter (γ) and Stretching sheet parameter (n).
- Temperature profiles are decrease for increasing Thermophoresis (Nt) and Brownian motion (Nb).
- The concentration reduces with increase in Brownian motion (*Nb*) and Lewis number (*Le*).
- In this study, the mathematical techniques utilised to solve the current physical model exhibit good agreement with prior existing research, indicating that the present physical findings are legitimate. In order to ensure validity, the findings are also compared with previously published results, which are found to be in fairly good agreement.

References:

- [1] H. Jeffreys. (1929). The Earth (fourth ed.), Cambridge University Press, London.
- [2] K. Vajravelu, K. V. Prasad, P. S. Datti and B.T. Raju. (2017). Convective flow, heat and mass transfer of Ostwald-de Waele fluid over a vertical stretching sheet, J. King Saud University Engineering Sciences, 29 (1), pp. 57-67.
- [3] P. V. Narayana, D. Babu and B. Venkateswarlu. (2017). Soret and Dufour effects on MHD radiative heat and mass transfer flow of a Jeffrey fluid over a stretching sheet, Frontiers in Heat and Mass Transfer (FHMT), 8.
- [4] S. Jena, S. R. Mishra and G. C. Dash. (2017). Chemical reaction effect on MHD Jeffery fluid flow over a stretching sheet through porous media with heat generation/absorption, Int. J. Algorithm. Comput. Math., 3 (2), pp. 1225-1238.
- [5] K. Sreelakshmi, G. Sarojamma and J. V. Murthy. (2018). Homotopy analysis of an unsteady flow heat transfer of a Jeffrey nanofluid over a radially stretching convective surface, J. Nanofluids, 7 (1), pp. 62-71.
- [6] K. Ahmad, Z. Hanouf and A. Ishak. (2016). Mixed convection Jeffrey fluid flow over an exponentially stretching sheet with magnetohydrodynamic effect, AIP Adv., 6 (3), Article 035024.
- [7] K. Das, N. Acharya and P. K. Kundu. (2015). Radiative flow of MHD Jeffrey fluid past a stretching sheet with surface slip and melting heat transfer, Alex. Eng. J., 54, pp. 815-821.
- [8] Z. Shafique, M. Mustafa and A. Mushtaq. (2016). Boundary layer flow of maxwell fluid in rotating frame with binary chemical reaction and activation energy, Results Phys., 6, pp. 627-633.
- [9] T. Hayat, M. Waqas, S. A. Shehzad and A. Alsaedi. (2015). MHD stagnation point flow of Jeffrey fluid by a radially stretching surface with viscous dissipation and joule heating, Journal of Hydrology and Hydromechanics, 63, pp. 311-317.
- [10] S. A. Shehzad, F. E. Alsaadi. (2013). S. J. Monaquel and T. Hayat, Soret and Dufour effects on the stagnation point flow of Jeffrey fluid with convective boundary condition, The European Physical Journal Plus, 128, p. 56.
- [11] F. M. Abbasi, S. A. Shehzad, T. Hayat, A. Alsaedi and M. A. Obid. (2015). Influence of heat and mass flux conditions in hydromagnetic flow of Jeffrey nanofluid, AIP Adv., 5, Article 037111.
- [12] D. Tripathi, N. Ali, T. Hayat, M. K. Chaube and A. A. Hendi. (2011). Peristaltic flow of MHD Jeffrey fluid through a finite length cylindrical tube, Appl. Math. Mech., 32, pp. 1148-1160.

ISSN: 1074-133X Vol 31 No. 4s (2024)

- [13] M. Farooq, A. Alsaedi and T. Hayat. (2015). Note on characteristics of homogeneous-heterogeneous reaction in flow of Jeffrey fluid, Appl. Math. Mech., 36, pp. 1319-1328.
- [14] N. A. M. Zin, I. Khan, S. Shafie and A. S. Alshomrani.(2017). Analysis of heat transfer for unsteady MHD free convection flow of rotating Jeffrey nanofluid saturated in a porous medium, Results in Physics, 7, pp. 288-309.
- [15] T. Hayat, M. Waqas, M. Ijaz Khan and A. Alsaed. (2017). Impacts of constructive and destructive chemical reactions in magnetohydrodynamic (MHD) flow of Jeffrey liquid due to nonlinear radially stretched surface, J. Mol. Liq., 225, pp. 302-310.
- [16] M. Ramzan, M. Bilal and J. D. Chung. (2017). Effects of thermal and solutal stratification on Jeffrey magnetonanofluid along an inclined stretching cylinder with thermal radiation and heat generation/absorption, Int. J. Mech. Sci., 131-132, pp. 317-324.
- [17] H. Shifang and K. G. Roesner. (1992). Time-dependent flow of upper-convected Jeffrey fluid between two rotating cylinders, Theoretical and applied rheology, pp. 216-218.
- [18] T. Hayat, S. Qayyum, M. Imtiaz and A. Alsaedi. (2017). Homogeneous-heterogeneous reactions in nonlinear radiative flow of Jeffrey fluid between two stretchable rotating disks, Results in Physics, 7, pp. 2557-2567.
- [19] P. V. S. Narayana and D. H. Babu. (2016). Numerical study of MHD heat and mass transfer of a Jeffrey fluid over a stretching sheet with chemical reaction and thermal radiation, J. Taiwan Inst. Chem. Eng., 59, pp. 18-25.
- [20] T. Hayat, M. Javed, M. Imtiaz and A. Alsaedi. (2017). Convective flow of Jeffrey nanofluid due to two stretchable rotating disks, J. Mol. Liq., 240, pp. 291-302.
- [21] P. Rana and R. Bhargava. (2012). Flow and heat transfer of a nanofluid over a nonlinearly stretching sheet: A numerical study, Commun. Nonlinear Sci. Numer. Simulat., 17 pp. 212-226.
- [22] S. Nadeem and N. S. Akbar. (2009).s Peristaltic Flow of a Jeffrey Fluid with Variable Viscosity in an Asymmetric Channel, Z. Naturforsch., 64a, 713-722.